Constrained Control Design for Magnetic Bearing Systems

Tingshu Hu[1], Zongli Lin[1], Wei Jiang[2], Paul E. Allaire[2]

[1] Department of Electrical and Computer Engineering
[2] Department of Mechanical and Aerospace Engineering
University of Virginia
P. O. Box 400743
Charlottesville, VA 22904-4743, USA.
Email: th7f, zl5y, wj2b, pea@virginia.edu

Abstract

We study the control problems in magnetic bearing systems that are subject to both input and state constraints. Apart from the usual restrictions on voltages and currents in the circuit systems, most magnetic bearing systems are subject to severe state constraint: the motion of the rotor (the suspended object) is only allowed in an extremely small air gap, otherwise the collision of the rotor and the stator would cause severe damages. Traditional methods for avoiding collision include increasing the air gap and increasing the currents, which usually result in unnecessarily large capacity of power supply and power loss. This paper presents a systematic approach to dealing with all the input and state constraints by using some recently developed tools for constrained control design. We hope that by dealing with the constraints properly, safety operation can be ensured with relatively small currents and power consumption. Experiment on the balance beam test rig in our laboratory shows that the design techniques are very effective.

Keywords: Constrained control, linearization, magnetic bearings, stabilization, transient performance

1 Introduction

Active magnetic bearings (AMB) have several appealing advantages over traditional bearings, such as very low power-loss, very long life, elimination of oil supply, low weight, reduction of fire hazard, vibration control and diagnostic capability[1]. They have been utilized in a variety of rotating machines ranging from artificial heart pumps, compressors, high speed milling spindles to flywheel energy storage systems. This work is intended to develop a systematic design approach to the control of magnetic bearing systems through a simple experimental setup at the University of Virginia. A key feature of our approach is that it takes state and control constraints into account in the design of feedback laws.

The experimental system we used in this paper is a beam balancing test rig (see Fig. 1 for a picture of the test rig and Fig. 2 for an illustrative diagram). It consists of a beam free to rotate on a pivot at its center of mass, and stabilized by electromagnets located at both

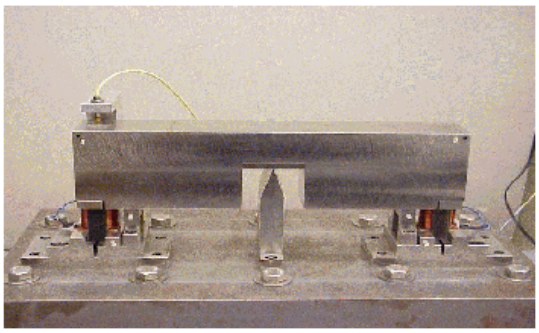

Figure 1: The beam balancing test rig.

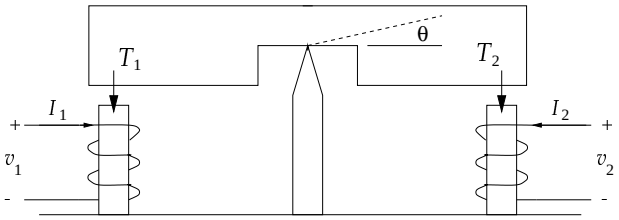

Figure 2: Illustrative diagram for the test rig.

ends of the beam. This experiment mimics the dynamics of a single axis AMB system. It captures the fundamental features of many magnetic bearing systems yet is quite simple from a mechanical viewpoint. Recently, in [5], we attempted to characterize the relationship between several performances and the biasing level through numerical optimization method.

The dynamics of the beam can be modeled by the following differential equation (see, e.g., [3]):

$$J\ddot{\theta} = -D\dot{\theta} + T_2 - T_1, \tag{1}$$

where θ is the angle between the beam and the horizontal direction, and T_1 and T_2 are the torques generated by the two electromagnets. The total torque provided by the electromagnets is $T_2 - T_1 =: T$. The system parameters are: J – the moment of mass, and D – system damping due to air and pivot friction.

The two electromagnetic circuits are described by the following differential equations:

$$L_1\dot{I}_1 = v_1 - I_1\dot{L}_1 - R_1 I_1, \tag{2}$$

$$L_2\dot{I}_2 = v_2 - I_2\dot{L}_2 - R_2 I_2, \tag{3}$$

where

$$L_1 = \frac{L_0 g_0}{g_0 + \theta}, \quad L_2 = \frac{L_0 g_0}{g_0 - \theta},$$

L_0 is the inductance of the coil when the beam is balanced ($\theta = 0$) and g_0 is the maximal angle which is reached when one end of the beam touches an electromagnet. The torques are

determined from the air gap fluxes in terms of I_1, I_2 and θ as follows,

$$T_1 = c_{t1}\left(\frac{g_0 I_1}{g_0+\theta}\right)^2, \quad T_2 = c_{t2}\left(\frac{g_0 I_2}{g_0-\theta}\right)^2,$$

where c_{t1} and c_{t2} are constants. In our test rig, $R_1 = R_2 = R$ and $c_{t1} = c_{t2} = c_t$.

Different magnetic bearing systems can be modeled similarly to the above balance beam system. For example, [8] considered a rotor whose one dimensional position is controlled by a pair of electromagnets. The model in [8] is mathematically the same as the one in this paper. Similar models were studied in [4], [9], etc. More complicated magnetic bearings are composed of several pairs of electromagnets as modeled above.

The magnetic bearing system (1)-(3) is a control system subject to both input and state constraints. First, the voltage supplies are always bounded, so we have $|v_1|, |v_2| \leq v_M$, for some v_M. The relation between the bound on the voltages and the performances of magnetic bearings has been studied in [12]. Second, the currents I_1 and I_2 are restricted within certain bound I_M to prevent over heating (or excessive power-loss) and flux saturation. Finally but most importantly, the displacement θ must be kept within $|\theta| \leq g_0$ to prevent the contact of the beam with the stator. The state constraints are often the most severe and must be observed. In rotational machinery suspended by magnetic bearing, the rotor may spin at a very high speed (e.g., the high speed flywheel energy storage system) and may have sharp blades on it (e.g., the artificial heart pump). The collision of the rotor and the stator will cause severe damage to the whole system. A factor that makes the control design even more difficult is that the displacement of the rotor is restricted to an extremely small value due to the usually very small air gap.

It appears to us that these constraints in the magnetic bearing systems have not been addressed systematically in the literature and in the industry. Although the voltage bound and the current bound can be selected according to the required force slew rate, the load tolerance and other performance requirements through estimation, this selection could be conservative and could lead to over-sized power supply. The state constraint, as far as we know, has not been paid sufficient attention. A common strategy is to restrict the motion of the rotor to a small portion of the air gap. This generally would result in an unnecessarily large air gap and hence unnecessarily large currents. We hope that, by dealing with all these constraints properly, the rotor could be allowed to move in the full air gap without causing collision and the currents and the capacity of power supply could be reduced considerably.

Recently, we developed a set of analysis and design tools to deal with input constraints (or actuator saturation) in control systems. These results are contained in the book [6]. In this paper, we will extend these results and develop some tools to deal with both input and state constraints in magnetic bearing systems. To use these tools, we need to obtain a linearized model. There are different ways to linearize a magnetic bearing system, including Jacobian linearization, feedback linearization and other approaches (see, e.g., [9, 10]). We first adopt the

conventional Jacobian linearization approach and will explain through stability analysis why it only works well under a large bias current. We will then present an exact linearization approach based on a nonlinear current allocation. We also present an almost linearization approach for the voltage mode. It appears that, among these three linearization methods, the exact linearization approach will lead to the best results: full utilization of the air gap, small bias current and robustness. All the results are verified on the balance beam test rig in our laboratory.

The remainder of the paper is organized as follows. In Section 2, we present some design tools for linear systems with input and state constraints, including stabilization and performance improvement. Section 3 designs controllers to enlarge the stability region through three linearization approaches. These three design approaches are compared through theoretical analysis and experimental verification. Section 4 addresses the issue of improving the transient performances. The effectiveness of the design techniques are also illustrated by experimental results. Section 5 concludes the paper.

Notation: For a real vector u, denote $|u|_\infty = \max_i |u_i|$. We use sat : $\mathbf{R}^m \to \mathbf{R}^m$ to denote the standard vector-valued saturation function, i.e., for $u \in \mathbf{R}^m$, the ith component of $\text{sat}(u)$ is $\text{sign}(u_i)\min\{1, |u_i|\}$.

2 Tools for constrained control design

Virtually all control systems are subject to input saturation and state constraint. In a magnetic bearing system, the control inputs are voltages or currents. The voltage supplies are always bounded and the currents are restricted within certain bounds to avoid flux saturation and over heating. The displacement of the suspended object are usually restricted to a very small value due to the usually small air gap. In this section, we develop some design tools to deal with the input and state constraints by extending some of the results in [6].

2.1 Systems with input and state constraints

Consider a linear system subject to input saturation and state constraint

$$\dot{x} = Ax + Bu, \quad x \in \mathbf{R}^n, \quad u \in \mathbf{R}^m. \tag{4}$$

The input constraint is imposed as $|u|_\infty \le 1$ and the state constraint is $x \in X_c$, where $X_c \subset \mathbf{R}^n$ is usually a polytope containing the origin in its interior. Our objective in this paper is to design a feedback law such that the closed-loop system possesses a large stability region and a good transient response. To design a feedback law such that the closed-loop system has a large stability region, we may construct a large invariant set, usually an invariant ellipsoid, that is inside the stability region.

An ellipsoid is associated with a positive definite matrix $P \in \mathbf{R}^{n\times n}$ ($P > 0$). Given a $P > 0$,

define the Lyapunov function as $V(x) = x^{\mathrm{T}} P x$ and denote

$$\mathcal{E}(P) := \{x \in \mathbf{R}^n : \quad x^{\mathrm{T}} P x \leq 1\}.$$

We are interested in the control of system (4) by saturated linear feedback of the form $u = \mathrm{sat}(Fx)$. The closed-loop system under this feedback law is

$$\dot{x} = Ax + B\mathrm{sat}(Fx). \tag{5}$$

An ellipsoid $\mathcal{E}(P)$ is invariant for system (5) if and only if

$$\dot{V}(x) = 2x^{\mathrm{T}} P(Ax + B\mathrm{sat}(Fx)) \leq 0, \quad \forall\, x \in \partial\mathcal{E}(P).$$

In this case, all the trajectories starting from $\mathcal{E}(P)$ will stay inside it. If we further have

$$\dot{V}(x) = 2x^{\mathrm{T}} P(Ax + B\mathrm{sat}(Fx)) \leq -\beta x^{\mathrm{T}} P x, \quad \forall\, x \in \mathcal{E}(P),$$

for some positive number β, then all the trajectories starting from $\mathcal{E}(P)$ will stay inside and converge to the origin. The number β can be considered as an indication of the convergence rate of the trajectories. A larger β usually results in good transient performances: fast response and small overshoot.

For a matrix $F \in \mathbf{R}^{m\times n}$, denote

$$\mathcal{L}(F) := \{x \in \mathbf{R}^n : \quad |Fx|_\infty \leq 1\}.$$

If the feedback control is $u = \mathrm{sat}(Fx)$, then $\mathcal{L}(F)$ is the region where u is linear in x. For simplicity, we assume that the state constraint set is a symmetric polytope,

$$X_c = \{x \in \mathbf{R}^n : \quad |Gx|_\infty \leq 1\} = \mathcal{L}(G),$$

for some matrix $G \in \mathbf{R}^{p\times n}$. To ensure that the state constraint $x \in \mathcal{L}(G)$ is satisfied all the time, we can construct an invariant ellipsoid $\mathcal{E}(P)$ such that $\mathcal{E}(P) \subset \mathcal{L}(G)$.

2.2 Design for large stability region

For any F such that $A + BF$ is Hurwitz, it is easy to see that the closed-loop system is locally asymptotically stable. In the presence of state constraint, the stability region is the set of initial conditions from which the state trajectories will stay inside $X_c = \mathcal{L}(G)$ and converge to the origin. An approach to enlarge the stability region is to design an F such that (5) has a large invariant ellipsoid inside $\mathcal{L}(G)$. The largeness of an ellipsoid can be measured with respect of a group of reference points $x_1, x_2, \cdots x_\ell$, by the number α_R defined as follows:

$$\alpha_R(P) := \max\{\alpha > 0 : \quad \alpha x_i \in \mathcal{E}(P) \ \ \forall\, i\}.$$

For example, suppose that the state of the system in (1) is $x = \begin{bmatrix} \theta & \dot{\theta} \end{bmatrix}^{\mathrm{T}}$ and we would like to achieve stabilization for a large initial angular displacement. We can then choose $x_1 = \begin{bmatrix} 1 & 0 \end{bmatrix}^{\mathrm{T}}$.

The problem of searching for an F that maximizes the invariant ellipsoid can be described as the following optimization problem

$$\begin{aligned} & \sup_{P>0,F} \ \alpha \\ \text{s.t.} \quad & a) \ \ \alpha x_i \in \mathcal{E}(P), \quad i = 1, 2, \cdots, \ell, \\ & b) \ \ (A + BF)^{\mathrm{T}} P + P(A + BF) \leq -\beta P, \\ & c) \ \ \mathcal{E}(P) \subset \mathcal{L}(F), \\ & d) \ \ \mathcal{E}(P) \subset \mathcal{L}(G). \end{aligned} \tag{6}$$

Under constraints b) and c), $\mathcal{E}(P)$ is an invariant ellipsoid. Constraint d) guarantees that the state constraint is satisfied inside this ellipsoid. A positive β ensures a certain margin of stability.

The optimization problem (6) can be transformed into an LMI problem by using the tools developed in Chapters 7 and 8 of [6]. Introducing new variables $Q = P^{-1}$, $H = FQ$ and $\gamma = 1/\alpha^2$, the optimization problem can be equivalently written as

$$\begin{aligned} & \inf_{Q>0,H} \ \gamma \\ \text{s.t.} \quad & a) \ \ \begin{bmatrix} \gamma & x_i^{\mathrm{T}} \\ x_i & Q \end{bmatrix} \geq 0, \quad i = 1, 2, \cdots, \ell, \\ & b) \ \ QA^{\mathrm{T}} + AQ + H^{\mathrm{T}} B + BH \leq -\beta Q, \\ & c) \ \ \begin{bmatrix} 1 & h_j \\ h_j^{\mathrm{T}} & Q \end{bmatrix} \geq 0, \quad j = 1, 2, \cdots, m, \\ & d) \ \ g_k Q g_k^{\mathrm{T}} \leq 1, \quad k = 1, 2, \cdots, p, \end{aligned} \tag{7}$$

where h_j is the jth row of H and g_k is the kth row of G. The above problem can be solved efficiently with LMI toolbox in Matlab.

2.3 Design for performance improvement

As we will see in Example 2, Section 3.2, the controller designed by solving (6) may result in slow transient response of the closed-loop system. To improve the transient response, we may try to maximize the number β in (6b). Meanwhile, we would like to guarantee certain desired stability region, for example, to ensure that the invariant ellipsoid $\mathcal{E}(P)$ include some desired points, $x_1, x_2, \cdots x_\ell$.

The problem of performance improvement with guaranteed stability region can thus be described by the following optimization problem:

$$\sup_{P>0,F} \ \beta \tag{8}$$

$$\text{s.t.} \quad a)\ x_i \in \mathcal{E}(P),\ \ i = 1, 2, \cdots, \ell,$$
$$b)\ (A + BF)^{\mathrm{T}} P + P(A + BF) < -\beta P,$$
$$c)\ \mathcal{E}(P) \subset \mathcal{L}(G) \cap \mathcal{L}(F).$$

Like the optimization problem (6), this optimization problem can be transformed into an LMI problem.

The constraint $\mathcal{E}(P) \subset \mathcal{L}(F)$ indicates that $|Fx|_\infty \leq 1$ and hence $\mathrm{sat}(Fx) = Fx$ for all $x \in \mathcal{E}(P)$, which means that the system (5) operates linearly inside the ellipsoid. Because of this, we have $|Fx|_\infty < 1$ for almost all $x \in \mathcal{E}(P)$. This means that the control input is almost always below the saturation level. To fully explore the control effort, we may try to use a controller of the form

$$u = -\mathrm{sat}(kB^{\mathrm{T}} Px). \tag{9}$$

Theoretically, by letting $k \to \infty$, the convergence rate of the Lyapunov function $x^{\mathrm{T}} Px$ is optimized (see Chapter 11 of [6]). However, all the practical systems have measurement noise, i.e., what we use for feedback is $x + \eta$ rather than the exact x, and the feedback control u is actually $u = -\mathrm{sat}(kB^{\mathrm{T}} P(x + \eta))$. By increasing k, the effect of noise is also magnified, as we will see in Example 4, Section 4. If the noise is of high frequency and the state is close to the origin, excessively large k will cause the control to switch between 1 and -1 constantly, causing implementation problem. Hence it is important to choose a suitable k to achieve a desired convergence rate while keeping the effect of measurement noise acceptable.

2.4 Possible reduction of the actuator capacity

By solving the optimization problems (6) and (8), we obtain an invariant ellipsoid $\mathcal{E}(P) \subset \mathcal{L}(G) \cap \mathcal{L}(F)$. The set inclusion relations $\mathcal{E}(P) \subset \mathcal{L}(G)$ and $\mathcal{E}(P) \subset \mathcal{L}(F)$ are generally not equally tight. This means that there may exist $\beta_G, \beta_F \in (0, 1]$ such that $\mathcal{E}(P) \subset \beta_G \mathcal{L}(G)$ and $\mathcal{E}(P) \subset \beta_F \mathcal{L}(F)$. Certainly, at least one of β_G and β_F must be 1 by optimality. If $\beta_G < \beta_F = 1$, then the input constraint is tighter. If $\beta_F < \beta_G = 1$, then the state constraint is tighter, indicating that within the ellipsoid $\mathcal{E}(P)$, $|Fx| \leq \beta_F < 1$, hence the actuator capacity can be reduced. In the magnetic bearing systems, due to the extremely small air gap, we usually have a tighter state constraint than an input constraint. In that case, the size of the power supply can be reduced.

3 Stabilization

To use the design tools in Section 2, we need to obtain a linear model of the magnetic bearing system. There are different approaches to linearization. Beside the conventional Jacobian linearization, feedback linearization and other approaches have been developed recently [9, 10]. In

this section, we will present three linearization approaches and the corresponding constrained control designs.

3.1 The Jacobian linearization under the current mode

The dynamics of the beam balancing test rig under the current mode can be modeled by the following differential equation,

$$J\ddot{\theta} = -D\dot{\theta} + c_t \left(\left(\frac{g_0 I_2}{g_0 - \theta} \right)^2 - \left(\frac{g_0 I_1}{g_0 + \theta} \right)^2 \right), \tag{10}$$

where D, c_t and g_0 are constants and g_0 is the maximal angular displacement which is reached when the beam touches one of the electromagnets. So we have $|\theta| \leq g_0$. It is assumed that $|I_1|, |I_2| \leq I_M$ to avoid flux saturation and over heating of the coils.

In the current mode, a circuit feedback law has been designed such that the actual current will closely follow a reference signal. We assume that the circuit dynamics can be ignored and the difference between the actual I_1 and I_2 and the desired I_1 and I_2 is sufficiently small. In this case, we consider I_1 and I_2 as the control inputs.

3.1.1 The linearized model and the feedback law

In (10), the currents appear in the form of I_1^2 and I_2^2, which are highly nonlinear for a control system. A conventional way to reduce this nonlinearity is to introduce a bias current $I_b > 0$ and let I_1 and I_2 operate symmetrically around I_b, i.e.,

$$I_1 = I_b + I, \quad I_2 = I_b - I, \tag{11}$$

where I is used as a control input that produces a net torque on the beam. Because of the bounds on the currents, we impose the constraint $|I| \leq I_M - I_b$.

With I_1 and I_2 determined from (11), the dynamical relation between the input I and the output θ is,

$$J\ddot{\theta} = -D\dot{\theta} + c_t \left(\left(\frac{g_0 (I_b - I)}{g_0 - \theta} \right)^2 - \left(\frac{g_0 (I_b + I)}{g_0 + \theta} \right)^2 \right), \tag{12}$$

which is still a nonlinear system. Performing Jacobian linearization at $(\theta, \dot{\theta}) = (0, 0)$ and $I = 0$, we obtain

$$\begin{bmatrix} \dot{\theta} \\ \ddot{\theta} \end{bmatrix} = \begin{bmatrix} 0 & 1 \\ \frac{4c_t I_b^2}{J g_0} & -\frac{D}{J} \end{bmatrix} \begin{bmatrix} \theta \\ \dot{\theta} \end{bmatrix} + \begin{bmatrix} 0 \\ -\frac{4c_t I_b}{J} \end{bmatrix} I. \tag{13}$$

Denoting $x = \begin{bmatrix} \theta & \dot{\theta} \end{bmatrix}^{\mathrm{T}}$ and

$$A_L = \begin{bmatrix} 0 & 1 \\ \frac{4c_t I_b^2}{J g_0} & -\frac{D}{J} \end{bmatrix}, B_L = \begin{bmatrix} 0 \\ \frac{-4c_t I_b}{J} \end{bmatrix},$$

we obtain the linearized system

$$\dot{x} = A_L x + B_L I, \quad |I| \le I_M - I_b. \tag{14}$$

We notice that the open-loop linearized system (14) has an unstable pole since $\det(A_L) < 0$.

Usually, a saturated linear feedback law $I = (I_M - I_b)\,\mathrm{sat}(Fx)$ is adopted with F being designed based on the linearized model. The linearized closed-loop system is then given by

$$\dot{x} = A_L x + B_L (I_M - I_b)\,\mathrm{sat}(Fx). \tag{15}$$

Under the feedback law $I = (I_M - I_b)\,\mathrm{sat}(Fx)$, the actual nonlinear closed-loop system is

$$J\ddot{\theta} = -D\dot{\theta} + c_t \left(\left(\frac{g_0(I_b - (I_M - I_b)\,\mathrm{sat}(Fx))}{g_0 - \theta} \right)^2 - \left(\frac{g_0(I_b + (I_M - I_b)\,\mathrm{sat}(Fx))}{g_0 + \theta} \right)^2 \right). \tag{16}$$

Based on the linearized model (14), we use the method in Section 2.2 to design an F for enlarging the stability region. In the optimization problem (6), we may choose $\ell = 1$ and $x_1 = (1, 0)$. By solving (6), we will maximize the initial displacement of the beam which can be brought to the balance position. However, this only guarantees the stability of the linearized system (15). In what follows, we will examine how well the behavior of the linearized system (15) predicts that of the nonlinear system (16). In doing so, we will obtain some quantitative measure of the effect of the biasing current on the ability of the linearized model to predict the stability region of the original nonlinear system.

3.1.2 Stability analysis

The linearized model approximates the nonlinear system (12) very well when θ is close to zero. When θ is close to g_0, the nonlinearity gets stronger and usually causes the beam to hit one of the electromagnets and stay there. Experimental experience shows that for large I_b, it is easy to find an initial position such that the beam will be balanced by the controller. If I_b is too small, it is very hard to manipulate the beam (by hands) into a proper position so that it can be balanced by the controller. In what follows, we would like to explain this through stability analysis of the linearized closed-loop system (15) and the actual closed-loop system (16).

Example 1 The parameters of the balance beam test rig are:

$$J = 0.0948\mathrm{kgm}^2, \quad g_0 = 0.004\mathrm{rad}, \quad c_t = 0.1384\mathrm{Nm/A}^2.$$

We choose $I_M = 1\mathrm{A}$ and use the method in Section 2.2 to design feedback laws. We take $A = A_L$, $B = B_L(I_M - I_b)$, where B absorbs the actual bound on the input I. The state constraint $|\theta| \le 0.004$ is equivalent to $x \in \mathcal{L}(G)$ with $G = [1/0.004 \;\; 0]$. The controller will be of the form $I = (I_M - I_b)\,\mathrm{sat}(Fx)$. In solving (6), we set $\ell = 1$ and choose $x_1 = (1, 0)$. To ensure certain stability margin, we choose $\beta = 0.01$. We designed feedback laws for $I_b = 0.5\mathrm{A}$

and $I_b = 0.1$A. The actual stability region of the nonlinear closed-loop system (16) can be computed by numerical method, for example, by simulating the time responses under different initial conditions.

For $I_b = 0.5$A, the optimal solution to (6) is $\alpha = 0.0028$. The control law is

$$I = 0.5\,\mathrm{sat}(357.7337\theta + 16.4353\dot{\theta}),$$

and the invariant ellipsoid is $\mathcal{E}(P)$ with

$$P = 10^5 \times \begin{bmatrix} 1.2797 & 0.0588 \\ 0.0588 & 0.0062 \end{bmatrix}.$$

Fig. 3 plots the boundary of the estimated stability region of the linearized close-loop system (15) in dashed curve (the boundary of $\mathcal{E}(P)$) and the boundary of the actual stability region of the nonlinear closed-loop system (16) in solid curves. We see that the estimated stability region based on the linearized model is well inside the actual stability region of the nonlinear system and is a valid (though conservative) estimate.

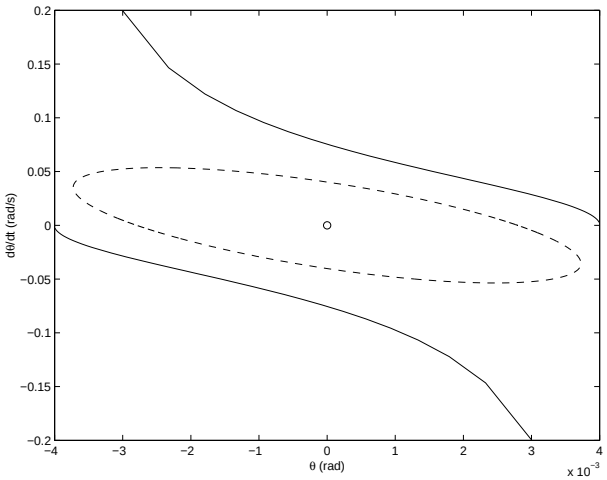

Figure 3: The stability region under $I_b = 0.5$A.

For $I_b = 0.1$A, the optimal solution to (6) is $\alpha = 0.004$. Notice that $g_0 = 0.004$rad. This means that the beam should be balanced from the initial position where the beam touches the electromagnets. The control law is

$$I = 0.9\,\mathrm{sat}(172.4701\theta + 9.8791\dot{\theta}),$$

and the invariant ellipsoid is $\mathcal{E}(P)$ with

$$P = 10^4 \times \begin{bmatrix} 6.2501 & 0.0016 \\ 0.0016 & 0.0859 \end{bmatrix}.$$

Fig. 4 plots the boundary of the estimated stability region of the linearized closed-loop system (15) in dashed curve and the boundary of the actual stability region of the nonlinear closed-loop system (16) in solid curves. In contrast to the case where $I_b = 0.5$A, most part of the estimated stability region is outside the actual stability region. This means that most initial conditions will lead to unstable response even if we predict a stable response based on the linearized model. For example, the beam will not be balanced by the controller if it is initially in touch with the electromagnets, as is verified by the experiment.

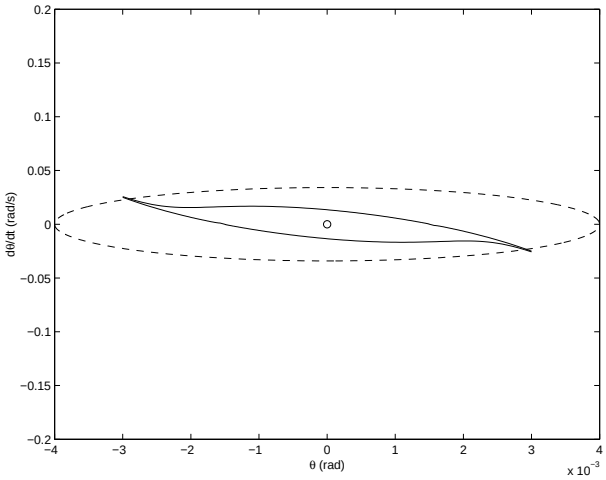

Figure 4: The stability region under $I_b = 0.1$

For comparison, we plot the boundary of the actual stability regions under $I_b = 0.1$A (in solid curves) and that under $I_b = 0.5$A (in dash-dotted curves) in Fig. 5. This explains why it is easier to balance the beam with a larger bias current. In the experiment, with $I_b = 0.5$A, the beam will be balanced even if it is initially in touch with one of the electromagnets. However, with $I_b = 0.1$A, it is very hard to manipulate the beam into an initial condition that can be balanced.

The above example shows that the relation between the estimated stability region of the linearized closed-loop system (15) and the actual stability region of the nonlinear closed-loop system (16) is quite complicated. The estimated stability region could be a subset of the actual stability region for large I_b. However, for small I_b, this relation does not hold. Because of this, it is hard achieve a large stability region by designing the stabilizing feedback law based on Jacobian linearization, especially when the bias current is small.

3.2 Exact linearization through nonlinear current allocation

The simple linear relation between I_1, I_2 and I in (11) results in a nonlinear dynamical relation (12) between I and θ. This makes it hard to design a stabilizing controller for small bias current.

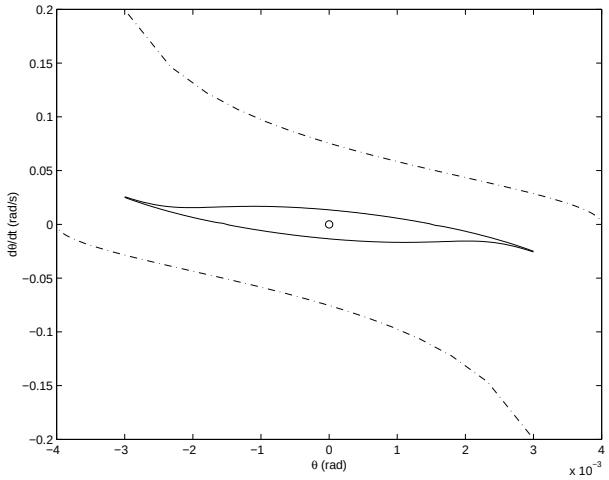

Figure 5: The stability regions under $I_b = 0.1$A and 0.5A

In this section, we use the following nonlinear current allocation strategy,

$$I_1 = (I_b + I)\frac{g_0 + \theta}{g_0}, \quad I_2 = (I_b - I)\frac{g_0 - \theta}{g_0}. \tag{17}$$

Under this nonlinear current allocation, the dynamical relation between I and θ is exactly linear:

$$J\ddot{\theta} = -D\dot{\theta} - 4c_t I_b I, \tag{18}$$

or,

$$\begin{bmatrix} \dot{\theta} \\ \ddot{\theta} \end{bmatrix} = \begin{bmatrix} 0 & 1 \\ 0 & -\frac{D}{J} \end{bmatrix} \begin{bmatrix} \theta \\ \dot{\theta} \end{bmatrix} + I_b \begin{bmatrix} 0 \\ -\frac{4c_t}{J} \end{bmatrix} I.$$

Denoting

$$A_E = \begin{bmatrix} 0 & 1 \\ 0 & -\frac{D}{J} \end{bmatrix}, \quad B_E = \begin{bmatrix} 0 \\ -\frac{4c_t I_b}{J} \end{bmatrix},$$

we have

$$\dot{x} = A_E x + B_E I, \quad |I| \le I_M/2 - I_b, \tag{19}$$

where the bound on I is imposed to guarantee that $|I_1|, |I_2| \le I_M$. We also note that there is no problem in generating the currents given by (17) since the values of $\frac{g_0 \pm \theta}{g_0}$ are between 0 and 2 ($|\theta| \le g_0$).

The system (19) is not only linear, but also marginally stable with one open-loop pole at 0 and another one at $-D/J$.

In this section, we consider the problem of stabilizing system (19) in the presence of state and input constraints. The performance issue will be addressed in Section 4.

Let the feedback law be of the form

$$I = (I_M/2 - I_b)\,\mathrm{sat}(Fx), \tag{20}$$

then the closed-loop system is

$$\dot{x} = A_E x + B_E(I_M/2 - I_b)\,\mathrm{sat}(Fx). \tag{21}$$

We also use the method in Section 2.2 to find a large invariant ellipsoid $\mathcal{E}(P)$ by solving (6) with $A = A_E$, $B = B_E(I_M/2 - I_b)$, $x_1 = (1, 0)$ and $\beta = 0.01$. Different from the design result in Section 3.1 for Jacobian linearization, in the case of exact linearization, $\mathcal{E}(P)$ is always inside the actual stability region. In what follows, we use an example to compare the invariant ellipsoid $\mathcal{E}(P)$ and the actual stability region. It turns out that $\mathcal{E}(P)$ is a good estimate of the actual stability region. Unlike with the Jacobian linearization, where $\mathcal{E}(P)$ could be an over estimate the actual stability region, here the linearization is exact and $\mathcal{E}(P)$ is always inside the actual stability region.

Example 2 Consider the same experimental system as in Example 1. Here we take $I_M = 2$A. For $I_b = 0.5$A, the optimal solution is $\alpha = 0.004$ and the controller is

$$I = 0.5\,\mathrm{sat}(179.9578\theta + 6.2261\dot{\theta}).$$

The invariant ellipsoid is $\mathcal{E}(P)$ with

$$P = 10^4 \times \begin{bmatrix} 6.2502 & 0.0010 \\ 0.0010 & 0.0238 \end{bmatrix}.$$

Fig. 6 plots the boundary of $\mathcal{E}(P)$, the estimated stability region, in dashed curve and the boundary of the actual stability region in solid curve.

For $I_b = 0.1$A, the optimal solution is also $\alpha = 0.004$ and the controller is

$$I = 0.9\,\mathrm{sat}(180.3603\theta + 10.3037\dot{\theta}). \tag{22}$$

The invariant ellipsoid is $\mathcal{E}(P)$ with

$$P = 10^4 \times \begin{bmatrix} 6.2502 & 0.0018 \\ 0.0018 & 0.0649 \end{bmatrix}.$$

Fig. 7 plots the boundary of $\mathcal{E}(P)$ in dashed curve and the boundary of the actual stability region in solid curve.

From Fig. 7, we see that the beam can be stabilized from initially touching the electromagnets, even with $I_b = 0.1$A. This result has been verified experimentally. The plots in Fig. 8 are the time responses under a bias current $I_b = 0.5$A and the plots in Fig. 9 are the time responses under $I_b = 0.1$A, all obtained from experimental data. The first plots in Figs. 8 and 9 are the time responses of the beam angle. The second and the third plots are the time responses of the currents I_1 and I_2. They were produced by pushing the beam to touch one of the electromagnets and then letting it go. After the steady state had been reached, the beam was pushed to touch

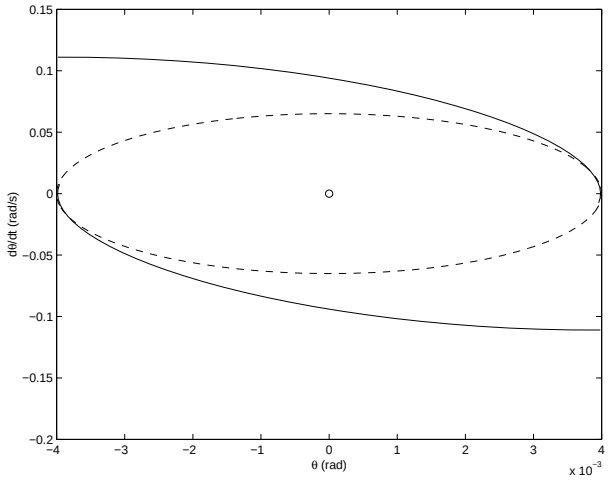

Figure 6: The estimated stability region and the actual stability region: $I_b = 0.5$A

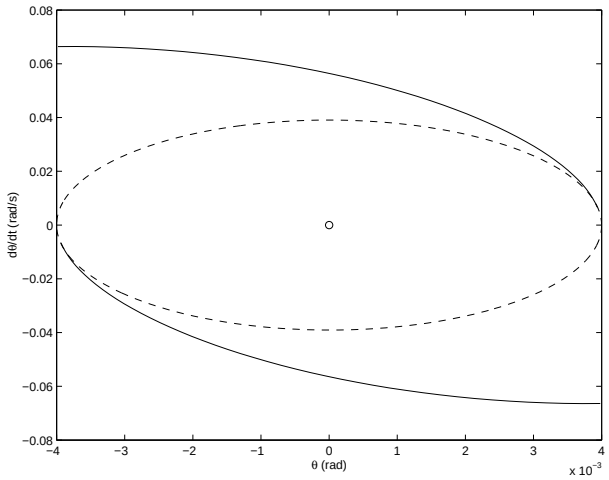

Figure 7: The estimated stability region and the actual stability region: $I_b = 0.1$A

the other electromagnet. This procedure was repeated several times for each set of the plots. As we can see, the beam always went back to the balance position. This was impossible with a bias current $I_b = 0.1$A under the controller based on the Jacobian linearization (13).

Experimental experience shows that the system is very robust against parameter uncertainties and disturbances even with $I_b = 0.1$A. For example, we incorporated uncertain gains k_1 and k_2, and some drift in the actuators so that the currents are

$$I_1 = k_1(I_b + I)\frac{g_0 + \theta}{g_0} + I_{10}, \quad I_2 = k_2(I_b - I)\frac{g_0 - \theta}{g_0} + I_{20}. \tag{23}$$

We tried with $(k_1, k_2, I_{10}, I_{20}) = (1, 1, -0.028, 0.05)$ and $(k_1, k_2, I_{10}, I_{20}) = (0.8, 1.2, 0, 0)$, respectively. The time responses of the beam angle are shown in Fig. 10, where the first plot corresponds to $(k_1, k_2, I_{10}, I_{20}) = (1, 1, -0.028, 0.05)$ and the second corresponds to $(k_1, k_2, I_{10}, I_{20}) =$

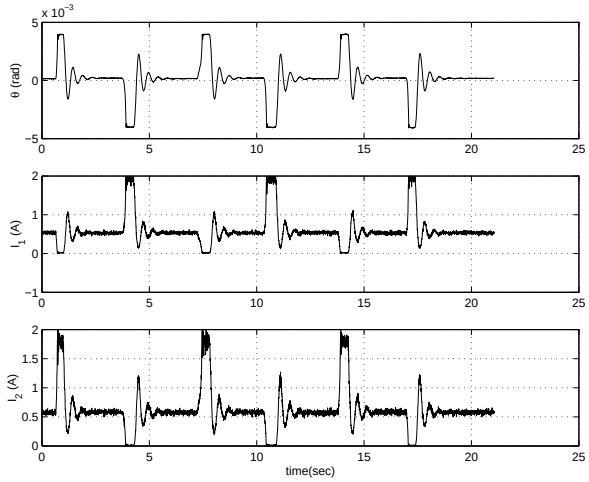

Figure 8: Experimental results: the time responses under $I_b = 0.5$A.

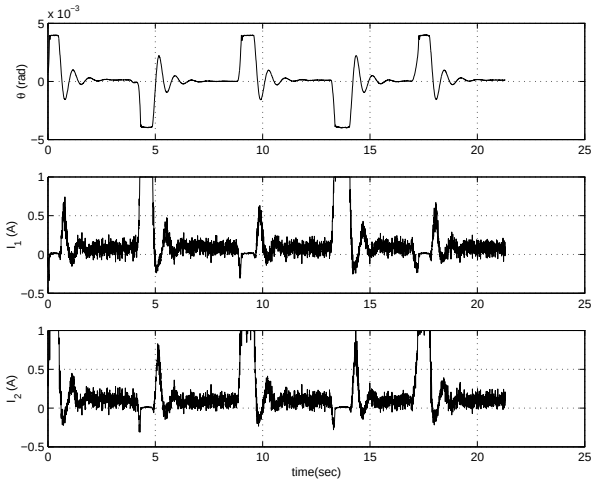

Figure 9: Experimental results: the time responses under $I_b = 0.1$A.

$(0.8, 1.2, 0, 0)$. We see that the stability is maintained under these parameter changes. The transient performances are slightly different. The overshoot from one side is larger than that from the other side.

3.3 The voltage mode: almost linearization

In the voltage mode, the currents are determined by the voltages in the circuit systems

$$L_1\dot{I}_1 = v_1 - I_1\dot{L}_1 - RI_1, \tag{24}$$

$$L_2\dot{I}_2 = v_2 - I_2\dot{L}_2 - RI_1, \tag{25}$$

where

$$L_1 = \frac{g_0}{g_0+\theta}L_0, \quad L_2 = \frac{g_0}{g_0-\theta}L_0.$$

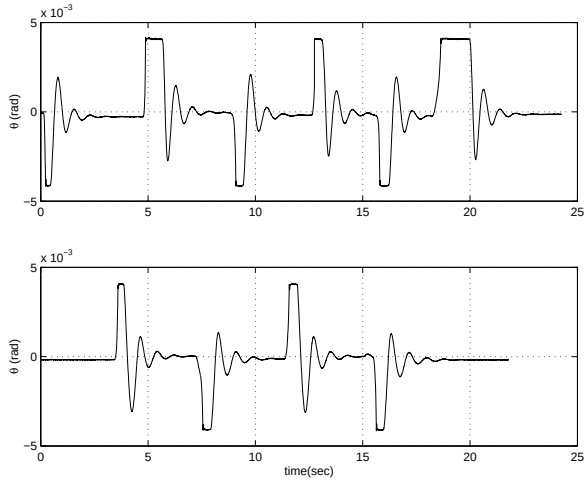

Figure 10: Experimental results: time responses under parameter changes for $I_b = 0.1$A: $(k_1, k_2, I_{10}, I_{20}) = (1, 1, -0.028, 0.05)$ and $(k_1, k_2, I_{10}, I_{20}) = (0.8, 1.2, 0, 0)$.

In this section, we investigate the control design in the voltage mode, where the inputs are v_1 and v_2.

To deal with the nonlinearity in the system, we define some new input and state variables. Let

$$u_1 = v_1 - RI_1, \quad u_2 = v_2 - RI_2, \quad \phi_1 = \frac{g_0}{g_0 + \theta} L_0 I_1, \quad \phi_2 = \frac{g_0}{g_0 - \theta} L_0 I_2.$$

Then we have

$$\ddot{\theta} = -\frac{D}{J}\dot{\theta} + \frac{c_t}{JL_0^2}(\phi_2^2 - \phi_1^2), \tag{26}$$

$$\dot{\phi_1} = u_1, \tag{27}$$

$$\dot{\phi_2} = u_2. \tag{28}$$

In fact, ϕ_1 and ϕ_2 are the fluxes in the electromagnets. If we further define $\phi_b = (\phi_1 + \phi_2)/2$, $\phi = (\phi_2 - \phi_1)/2$, $w_1 = (u_2 - u_1)/2$ and $w_2 = (u_1 + u_2)/2$, we obtain

$$\ddot{\theta} = -\frac{D}{J}\dot{\theta} + \frac{4c_t}{JL_0^2}\phi_b\phi, \tag{29}$$

$$\dot{\phi} = w_1, \tag{30}$$

$$\dot{\phi_b} = w_2. \tag{31}$$

Notice that there is a bilinear term $\phi_b\phi$ in (29). Since ϕ_b is under the control of the input w_2 and is independent of other states, we can use a simple controller

$$w_2 = k_1(\phi_{bd} - \phi_b) \tag{32}$$

with a positive number k_1 to make ϕ_b approximate some constant ϕ_{bd}. After ϕ_b has reached a steady state, the other states $\theta, \dot{\theta}$ and ϕ and the input w_2 satisfy the following linear relation

$$\begin{bmatrix} \dot{\theta} \\ \ddot{\theta} \\ \dot{\phi} \end{bmatrix} = \begin{bmatrix} 0 & 1 & 0 \\ -\frac{D}{J} & 0 & \frac{4c_t}{JL_0^2}\phi_b \\ 0 & 0 & 0 \end{bmatrix} \begin{bmatrix} \theta \\ \dot{\theta} \\ \phi \end{bmatrix} + \begin{bmatrix} 0 \\ 0 \\ 1 \end{bmatrix} w_1. \tag{33}$$

For the above system, a simple linear feedback law of the form

$$w_1 = k_2\theta + k_3\dot{\theta} + k_4\phi \tag{34}$$

can be designed to meet certain performance and stability requirements.

The closed-loop system (29)-(31), (32) and (34) is not strictly linear because of the bilinear term $\phi_b\phi$. The transient dynamics of ϕ_b can be considered as causing a finite energy disturbance $\frac{4c_t}{JL_0^2}(\phi_b - \phi_{bd})\phi$ and the whole system is stable. If the control law (34) has certain degree of robustness and if the dynamics of ϕ_b is fast, then the performances of the whole system will be close to those of the linear system (33)-(34).

It should be noted that the idea of obtaining a linear system by setting the sum of the fluxes fixed is similar to that in [9]. Different from [9], here we take the voltages as inputs and the dynamics of the fluxes is considered. Moreover, we will also address all the input and state constraints in our consideration.

From the feedback laws (32) and (34), the feedback relation between the original states $(\theta, \dot{\theta}, I_1, I_2)$ and inputs (v_1, v_2) can be obtained as follows

$$\begin{aligned} v_1 &= RI_1 + u_1 \\ &= RI_1 + w_2 - w_1 \\ &= RI_1 + k_1(\phi_{bd} - \frac{\phi_1 + \phi_2}{2}) - k_2\theta - k_3\dot{\theta} - k_4\frac{\phi_2 - \phi_1}{2} \\ &= -k_2\theta - k_3\dot{\theta} + \left(R + \frac{(k_4 - k_1)g_0L_0}{2(g_0 + \theta)}\right) I_1 - \frac{(k_4 + k_1)g_0L_0}{2(g_0 - \theta)} I_2 + k_1\phi_{bd}, \end{aligned} \tag{35}$$

and

$$\begin{aligned} v_2 &= RI_2 + u_2 \\ &= RI_2 + w_2 + w_1 \\ &= RI_2 + k_1(\phi_{bd} - \frac{\phi_1 + \phi_2}{2}) + k_2\theta + k_3\dot{\theta} + k_4\frac{\phi_2 - \phi_1}{2} \\ &= k_2\theta + k_3\dot{\theta} - \frac{(k_4 + k_1)g_0L_0}{2(g_0 + \theta)} I_1 + \left(R + \frac{(k_4 - k_1)g_0L_0}{2(g_0 - \theta)}\right) I_2 + k_1\phi_{bd}. \end{aligned} \tag{36}$$

To satisfy the voltage bound, we may assign a bound to each item RI_1, RI_2, w_1 and w_2. The bounds on RI_1 and RI_2 can be computed from the bounds on the currents, $|I_1|, |I_2| \leq I_M$. Let the bounds on w_1 and w_2 be w_{1M} and w_{2M}, and let the maximal value of the voltage supply be v_M, then we need to choose $w_{1M}$and w_{2M} such that $w_{1M} + w_{2M} + RI_M \leq v_M$.

The bias flux ϕ_{bd} corresponds to a bias current $I_b = \phi_{bd}/L_0$ at steady state. The bounds on the currents impose a bound on the flux as $|\phi_1|, |\phi_2| \le L_0 I_M/2$, so we need to restrict ϕ such that $|\phi| \le L_0(I_M/2 - I_b)$.

In summary, for (33), we need to consider the following state and input constraints,

$$|\theta| \le \theta_M, \quad |\phi| \le L_0(I_M - I_b), \quad |w_1| \le w_{1M}.$$

In order to design the control law (34), we may set the objective as finding the invariant ellipsoid $\mathcal{E}(P)$ that contains $\alpha[1 \;\; 0 \;\; 0]^{\mathrm{T}}$ with α maximized. This will result in the largest initial displacement of the beam that can be brought back to the balance position. This objective can be easily transformed into the optimization problem (6), which can be solved efficiently.

As to the design of the control law (32), suppose that the initial ϕ_b is 0, then $|\phi_{bd} - \phi_b| \le \phi_{bd}$ for all time. The constraint on w_2 can be easily satisfied by choosing k such that $k\phi_{bd} \le w_{1M}$.

Example 3 Consider the same balance beam test rig as in Example 1. The additional parameters in the circuit systems are

$$R = 0.7\Omega, \quad L_0 = 4.9060 \times 10^{-4} H.$$

We used PWM (pulse width modulated) power amplifier to provide a desired voltage. The voltage bound is $v_M = 15V$. We set $I_M = 2\mathrm{A}$, $w_{1M} = 10V$ and $w_{2M} = 3.6V$. We choose $\phi_{bd} = 0.1L_0$ and take $\beta = 4$ to ensure some stability margin. The optimal value of α is 0.0037 and the control law is,

$$w_1 = 10\,\mathrm{sat}(-38.6\theta - 4.6\dot{\theta} - 1353.9\phi), \quad w_2 = 50(\phi_{bd} - \phi).$$

For the closed-loop system (33) and (34), the point $(\theta, \dot{\theta}, \phi) = (0.0037, 0, 0)$ is in the resulting invariant ellipsoid $\mathcal{E}(P)$. Since $\mathcal{E}(P)$ could be conservative as an estimation of the stability region, we tried an initial state $(\theta, \dot{\theta}, \phi) = (0.00399, 0, 0)$ and simulation confirms that this point is still in the stability region. Fig. 11 plots the simulation results with initial conditions $(\theta, \dot{\theta}, \phi) = (0.00399, 0, 0)$ and $\phi_b = 0$.

From the simulation result, it is expected that the controller can bring the beam to the balance position from initially touching one of the electromagnets. However, we didn't do this successfully at the first trials on the experiment. Actually, we were unable to manipulate the beam into a position that could be stabilized. To find out the reason, we did some simulation by adding some disturbances to the voltage supply. Instead of letting $v_1 = RI_1 + w_2 - w_1$ and $v_2 = RI_2 + w_2 + w_1$ as in (35) and (36), we output

$$v_1 = RI_1 + w_2 - w_1 + v_{10}, \quad v_2 = RI_2 + w_2 + w_1 + v_{20}$$

from the controller. Fig. 12 plots the simulation results with $v_{10} = -0.02V$, $v_{20} = -0.01V$ and initial conditions $(\theta, \dot{\theta}, \phi, \phi_b) = (0, 0, 0, 0)$. Clearly, the time responses are diverging and indicate instability.

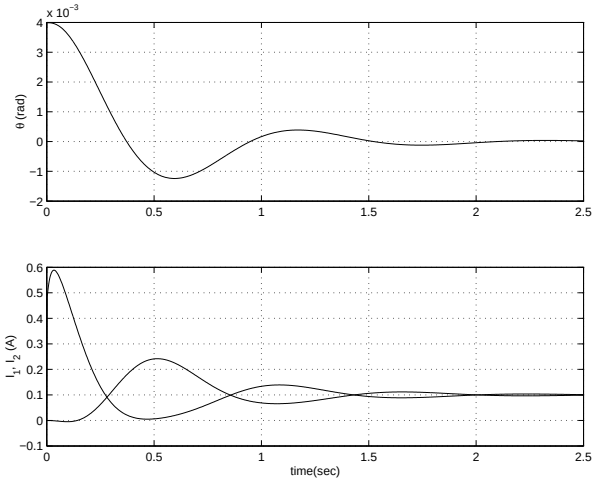

Figure 11: Simulation: a time response of the exact system

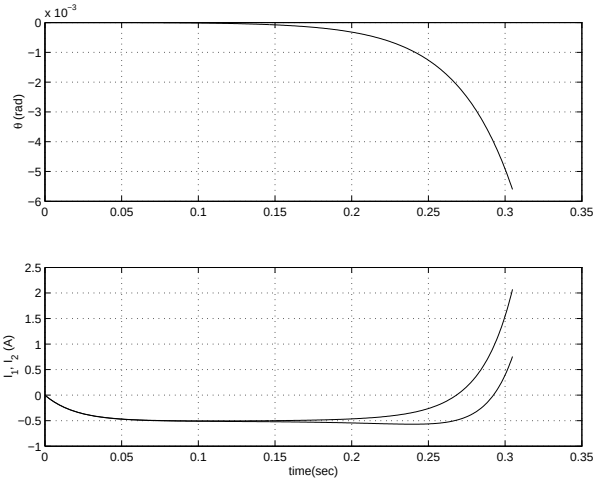

Figure 12: Simulation: unstable response under actuator uncertainties.

The simulation result thus shows that the control system is very sensitive to the voltage drift. The reason is that, in the control law (35) and (36), the term $k\phi_{bd}$ is very small. In the case $k = 50$ and $I_b = 0.1$, $k\phi_{bd} = 0.0025$. A small drift of the voltage would result in a large drift of the effective ϕ_{bd}. Recognizing this, we checked the drift of the voltages and made some correction. The behavior of the test rig was indeed improved. The first plot in Fig. 13 is the time response of the angle plotted from experimental data. The second and the third plots in Fig. 13 plot the currents I_1 and I_2. The beam went back to the balance position after every pushing to the electromagnets and releasing. However, the currents, which should be around 0.1A, were actually about $0.25A$ in the steady state. The deviation of the currents from the theoretical value is caused by the positive voltage drift. In fact, it is impossible to eliminate the voltage drift completely.

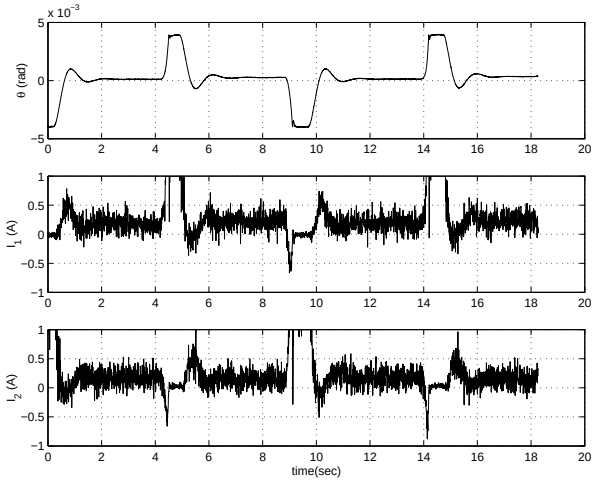

Figure 13: Experimental results: a stable time response

Since we used a PWM power amplifier, the currents are subject to severe disturbances. We can see from the plots in Fig. 13 that the disturbance is of very high frequency and large amplitude as compared to the actual current. However, this big disturbance does not seem to have a big influence on the performance of the test rig. This is because the mechanical system acts as a low-pass filter. The main disadvantage of the voltage mode is that it is very sensitive to actuator uncertainties. This is possibly caused by the PWM power amplifier.

4 Performance Improvement

We presented three approaches for stabilizing magnetic bearing systems in Section 3. From our experience with the experimental test rig, the exact linearization approach under the current mode exhibits the best properties in several important aspects including large stability region, robustness and disturbance rejection. In this section, we will focus on improving the transient performance for the exact linearized system under the current mode.

Section 2.3 presents an approach to improving the transient performance by solving the optimization problem (8). Two controllers can be constructed from the optimal solution:

$$u = \mathrm{sat}(Fx) \tag{37}$$

and

$$u = -\mathrm{sat}(kB^{\mathrm{T}}Px). \tag{38}$$

The gain k needs to be adjusted for the best results. In what follows, we use an example to illustrate the effectiveness of the design technique.

Example 4 Consider again the balance beam test rig. In solving the optimization problem (8), we choose $\ell = 1$ and $x_1 = \begin{bmatrix} 0.004 \\ 0 \end{bmatrix}$. The state constraint is represented by $\mathcal{L}(G)$ with $G = [1/0.004 \;\; 0]$. Here is the optimal solution for the case $I_b = 0.1$A:

$$\beta = 14.2229, \quad F = [144.3389 \;\; 27.0619], \quad P = \begin{bmatrix} 6.2500 & 0.5859 \\ 0.5859 & 0.0824 \end{bmatrix} \times 10^4.$$

Based on this solution, we obtained two controllers

$$I = 0.9\text{sat}(Fx) = 0.9\,\text{sat}(144.3389\theta + 27.0619\dot{\theta}), \tag{39}$$

and

$$I = 0.9\text{sat}(kB^{\mathrm{T}}Px) = 0.9\,\text{sat}(307.9317\theta + 43.3008\dot{\theta}). \tag{40}$$

Experimental results show that the performance of the balance beam is much improved by using the controllers (39) and (40). Fig. 14 compares the time responses of the angle under these controllers and that under the controller (22), where the dash-dotted curve corresponds to (22), the dashed curve to (39) and the solid curve to (40). The time response under (22) was plotted from $t = 0$ to $t = 4$, while the time responses under (39) and (40) were only plotted from $t = 0$ to $t = 2.5s$. This is because the steady state was reached much earlier under (39) and (40). already reached.

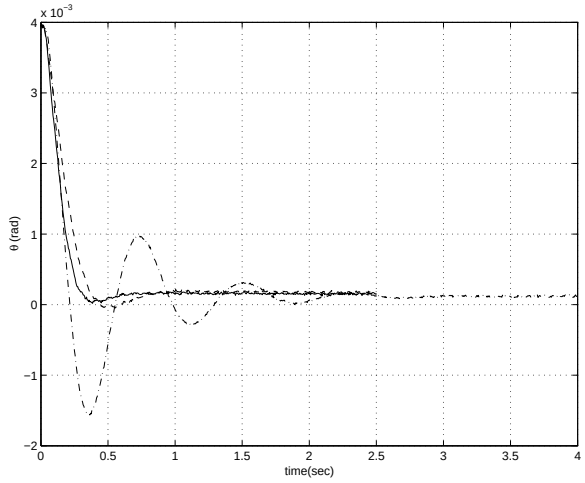

Figure 14: Experimental result: The time responses of θ under different control laws (22), (39) and (40).

Figs. 15 and 16 plot the time responses of the currents. In each figure, the first plot is the current under the controller (22), the second plot under (39) and the third plot under (40). In each plot, the average value of the currents are about 0.1A in the steady state. But the variation is larger under the controllers (39) and (40). The reason is that, in these two controllers, the

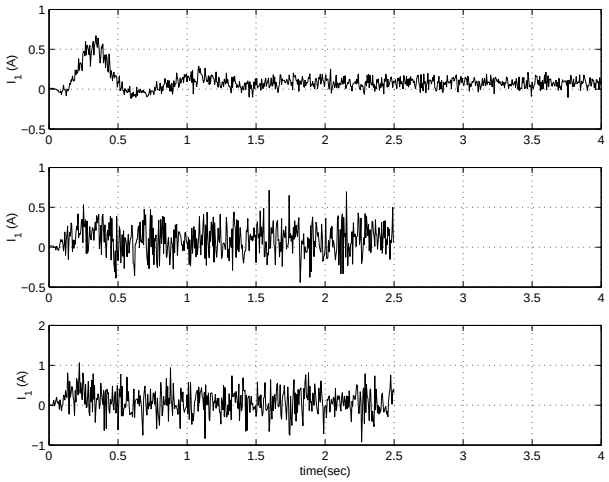

Figure 15: Experimental result: The time responses of I_1 under different control laws (22), (39) and (40).

coefficients of $\dot{\theta}$ are larger that that in (22) and the measurement of the rotational velocity is subject a larger disturbance than the measurement of the angle. If we increase the gain k in the controller (40), this disturbance will be amplified and result in larger variations of the currents. If the currents exceed the saturation level, then the performance and stability of the system cannot be guaranteed.

5 Conclusions

This paper developed a systematic control design approach for magnetic bearing systems which are subject to both input and state constraints. We extended some of our recently developed tools to design controllers for the purposes of enlarging the stability region and improving the transient performance. We investigated three design approaches through three different linearization methods and compared the stability performances under these approaches. It turned out that, among these three linearization methods, the exact linearization through nonlinear current allocation is the best approach. It results in large stability region, good robustness and disturbance rejection. As applied to the balance beam test rig, the designed controller allows full utilization of the air gap even with a small bias current. The technique for performance improvement has also proved to be very effective.

References

[1] P. E. Allaire, E. H. Maslen, R. R. Humphris, C. R. Knospe and D. W. Lewis, "Magnetic Bearings," in *CRC Handbook of Lubrication and Tribology*, Vol. 3, R. Booser, Ed., CRC Press.

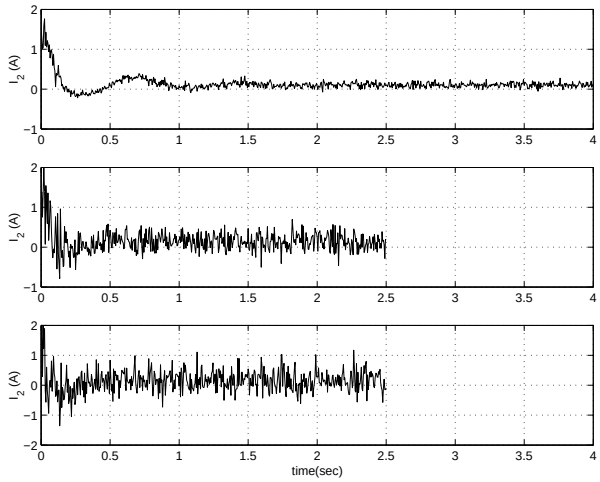

Figure 16: Experimental result: The time responses of I_2 under different control laws (22), (39) and (40).

[2] M. Baloh, "Practical concerns of linearizing AMB: power loss reduction, amplifier dynamics, and flux estimation," *Proceedings of the 6th International Symposium on Magnetic Suspension Technology (ISMST)*, pp.105-110, Turin, Italy, October, 2001.

[3] M. Baloh, "Time varying feedback linearization of magnetic bearing actuator," Ph. D Dissertation, University of Virginia, 2001.

[4] A. Charara, J. De Miras and B. Caron, "Nonlinear control of a magnetic levitation system without premagnetization," *IEEE Transaction on Control Systems Technology*, Vol. 4, No. 5, pp. 513-523, 1996.

[5] T. Hu, Z. Lin, B. Huang and P. E. Allarie, "On minimum current biasing and control for a balanced beam suspended on magnetic bearings," *Proceedings of the 6th International Symposium on Magnetic Suspension Technology (ISMST)*, pp.410-415, Turin, Italy, October, 2001.

[6] T. Hu and Z. Lin. *Control Systems with Actuator Saturation: Analysis and Design*, Birkhäuser, Boston, 2001.

[7] D. Johnson, G. V. Brown, D. I. Inman, "Adaptive variable bias magnetic bearing control," *Proceedings of the 1998 American Control Conference*, Philadelphia, PA, 1998.

[8] J. Levine, J. Lottin and J-C. Ponsart, "A nonlinear approach to the control of magnetic bearings," *IEEE Transaction on Control Systems Technology*, Vol. 4, No. 5, pp. 524-544, September, 1996

[9] L. Li, "Linearization of feedback actuators by constant current sum, constant voltage sum and constant flux sum," *IEEE Trans. on Magnetics*," Vol. 35, No. 1, 1999.

[10] L. Li and J. Mao, "Feedback linearization of magnetic bearing actuators for uniform upward bound of force slew rate, " *IEE Proc. Electrical Power Applications*," 146(4), 1999.

[11] F. Lösch, "Two remarks on the modeling of active magnetic bearing systems," *Proceedings of the 6th International Symposium on Magnetic Suspension Technology (ISMST)*, pp.422-427, Turin, Italy, October, 2001.

[12] E. H. Malsen, P. Hermann and M. Scott, "Practical limits to the performance of magnetic bearings: peak force, slew rate and displacement sensitivity," *ASME Journal on Tribology*, Vol. 111, pp. 331-336, 1989.